Catalysis Science & Technology

Accepted Manuscript

ROYAL SOCIETY OF CHEMISTRY

www.rsc.org/catalysis

Catalysis Science & Technology RSCPublishing

ARTICLE

An efficient route to prepare highly dispersed metallic copper nanoparticles on ordered mesoporous silica with outstanding activity for hydrogenation reactions

Cite this: DOI: 10.1039/x0xx00000x

Received 00th January 2012,
Accepted 00th January 2012

DOI: 10.1039/x0xx00000x

www.rsc.org/

Constantin Rudolf[a], Fatima Abi-Ghaida[b], Brindusa Dragoi[a], Adrian Ungureanu[a]*, Ahmad Mehdi[b]*, Emil Dumitriu[a],

Copper nanoparticles at relatively high metal loading of 10 wt. % were successfully synthesized via incipient wetness impregnation by using polyether-functionalized ordered mesoporous silica as organic-inorganic hybrid supports. The effect of functionalized triblock copolymer Pluronic P123 (0, 25 and 50 wt. % of total triblock copolymer in gel) on the structural and catalytic properties of copper nanocomposite materials was specifically investigated. The oxide forms of materials were systematically characterized by nitrogen physisorption, SAXS, WAXS, TEM, EDXS, DR UV-Vis and TPR, while the metallic forms were analysed by N_2O chemisorption, WAXS and TEM. The results indicated that the use of mesoporous silica hybrids leads to highly dispersed supported copper nanoparticles (dispersions in the range 43-57 %) displaying excellent activity in the hydrogenation of cinnamaldehyde. The average particle size was shown to decrease from 2.3 to 1.7 nm with the increase in the amount of functionalized triblock copolymer from 0 to 50 wt. %. Under standard test conditions, all the nanosized copper catalysts showed high catalytic activity but selectivity towards the saturated aldehyde. Further improvements in activity and selectivity towards the unsaturated alcohol were achieved by increasing the hydrogen pressure and applying a two-step reduction-oxidation pre-treatment, respectively. The structure and controllable properties of nanoscale copper materials developed herein, both oxidic and metallic forms, make them very attractive candidates for both fundamental research and practical catalytic applications.

Introduction

In the field of heterogeneous catalysis, the unique electronic structure and the high active surface of metal (oxide) nanoparticles (NPs) determine the selectivity and activity of catalysts. An extensive array of research was effectuated for the development of new heterogeneous catalysts with high performances and thus with great applicative potential in fine chemistry, petrochemistry, pollution prevention/control and other important fields.[1] For these applications, catalysts are usually formulated as metal (oxide) NPs deposited on inorganic or organic porous supports. Striking different catalytic properties have been reported for NPs as compared with the bulk counterparts. Particle size, geometry, composition, oxidation state, and chemical/physical environment play key roles in determining the performance of supported NPs.[2] For instance, one of the most interesting metals is copper, which is catalytically inactive in bulk form during hydrogenation reactions but becomes active when the particle size decreases to 10 nanometers or bellow.[3-9] As an example, commercial methanol synthesis catalysts typically consist of Cu nanoparticles (about 5-10 nm in size) spaced by smaller ZnO crystallites.[6,7] However, copper NPs are difficult to be stabilized, especially at high loading of copper on silica supports, due to the high mobility of copper species, resulting in significant sintering, even at low temperatures, and formation of undesired large agglomerates.[9]

Therefore, attempts have been made to disperse copper under the form of small particles by using mesoporous silica SBA-15 as supports based on some properties such as high hydrothermal stability, high surface area, and two-dimensional cylindrical pores.[9-11] Even though various strategies can be envisioned to obtain high dispersion and enhanced stability of copper NPs, such as deposition precipitation,[11, 12] precipitation,[11] wet impregnation,[11, 13] incipient wetness impregnation (IWI),[9] and IWI followed by mild drying IWI-MD,[4, 7] microwave irradiation assisted impregnation[10] and chemical reduction,[8] the impregnation routes remain simpler, less expensive and environmentally friendly. Moreover, functionalization of mesoporous surface by chelating groups like –COOH is often required to obtain a high dispersion of Cu NPs via impregnation with aqueous solution of copper nitrate.[13, 14] Alternatively, the hydrophobic core of the P123 surfactant micelle in the as-synthesized SBA-15 can be employed to entrap hydrophobic precursors of copper acetyl acetonate, resulting also in high dispersion of Cu NPs,[15] yet at less than 1 wt. % copper loading. From these recent studies, it is evident that the functionalization of mesoporous silica indeed offers specific tailoring of the surface chemical properties of support which improves the interaction between copper precursors and pore surfaces, finally leading to high dispersions of copper NPs stabilized within the pores of support.

Herein, we report a new route to prepare highly dispersed metallic copper nanoparticles on mesoporous silica at relatively high copper loading of 10 wt. %, based on the functionalization of mesoporous silica supports with polyether groups. First, a functionalized bis-silylated triblock copolymer Pluronic P123 (Si-P123) containing triethoxysilyl moieties at the chain ends was prepared, according to a previously reported procedure.[16] The functionalized triblock copolymer had thereafter two major roles: (i) as secondary structure direction agent (SDA) for the two-dimensional hexagonal SBA-15-like mesostructure containing functional polyether chains covalently bound to the silica framework where the primary SDA was the unfunctionalized P123 triblock copolymer, and (ii) as dispersing agent for the copper precursors impregnated as aqueous solutions into the support porosity. The polyether-functionalized mesoporous silica with controlled contents of covalently bound P123 presented enhanced capacity to stabilize copper precursors, thus explaining the high dispersion of copper (oxide) NPs achieved after surfactant removal by calcination under air, and reduction under hydrogen. As a result, the metal forms of catalysts manifested outstanding performances in cinnamaldehyde hydrogenation. This reaction is very interesting from a fundamental point of view (control of the chemoselectivity) and it has been extensively studied.[3, 17] Likewise, cinnamaldehyde hydrogenation is industrially relevant because the products of partial or total hydrogenation are being used in flavour and perfume industry, cosmetics, pharmaceutics etc. Consequently, a wide variety of efficient noble metal-based catalysts were reported for the hydrogenation of cinnamaldehyde, amongst which are platinum,[18-23] iridium,[24, 25] ruthenium,[26-28] and rhodium.[29] Albeit the cost-effective, nanosized copper-based catalysts have great potential to replace the expensive noble metal-base catalysts, they were seldom investigated in cinnamaldehyde hydrogenation.[8, 30, 31] For example, Guttierez et al. recently reported that the selectivity levels achieved over Cu/MCM-41 catalysts (20% metal loading, Cu NPs of 3.8 nm in size) are higher than those over noble metal-based catalysts (Au and Pt), under the same reaction conditions.[8]

Experimental

Synthesis of bis-silylated P123

Bis-silylated P123 (Si-P123) was synthesized according to Grandsire et al.[16] as follows: a solution of 10 g (1.72 mmol) of Pluronic P123 ($EO_{20}PO_{70}EO_{20}$, where EO = ethyleneoxide, PO = propyleneoxide; molecular weight of 5800; BASF Corp.) in CH_2Cl_2 (200 mL) was dried with magnesium sulphate and filtered. CH_2Cl_2 was removed and polymer was heated under vacuum at 100 ^oC for 12 h. Dry P123 was then silylated with 3-isocyanatopropyltriethoxysilane (ICPTES). To a solution of P123 (0.1 M) in dry THF (tetrahydrofuran,100 mL), an excess of ICPTES (4 equiv.) and Et_3N (triethylamine, 2 equiv.) were added at room temperature. The mixture was stirred at reflux for 72 h under argon. After removal of THF and Et_3N, the obtained crude was washed with pentane four times and dried, giving rise to 9.39 g (1.50 mmol, 87%) of Si-P123 as colourless oil.

Synthesis of functionalized supports and catalysts

For this study a series of supports were obtained based on a previous reported method.[16] The difference between them is the amount of Si-P123 used. All the supports were denoted as Mx, where "*M*" stands for mesoporous support and "*x*" stands for the mass percentage of Si-P123 used in gel (*x*, wt. % = $m_{Si\text{-}P123}/(m_{Si\text{-}P123}+m_{P123})$. The M0 support was prepared according to the following procedure. 8.2 g (1.36 mmol) of block copolymer P123 was solubilized in 300 mL of an aqueous HCl solution (pH = 1.5) in an Erlenmeyer flask. After 2-3 h of stirring, the solution was poured into another flask containing 18.7 g (89.78 mmol) of tetraethoxysilane at room temperature. The reaction medium was left for 2 h and 30 min at room temperature under regular magnetic stirring to give rise to a microemulsion; the solution appeared perfectly clear and colorless. The flask was immersed in an oil bath at 60 °C and after 2 min, 150 mg (3.6 mmol) of NaF was added under stirring to allow hydrolysis-polycondensation.[32] A white precipitate formed in a few minutes. The reaction mixture was left under stirring for 72 h at 60 °C, the resulting powder was filtered off and the unbound surfactant was removed by Soxhlet extraction over ethanol for 24h and then was dried at 120 ^oC under vacuum to give 5.6 g of M0 as white powder. For the synthesis of M25 and M50 supports, the same procedure was followed, apart from the amounts of Si-P123 and P123 used, as shown in Table 1.

Table 1. Amounts of bisilylated P123 and P123 used for supports synthesis

Sample / SDA	M0	M25	M50
m P123 (g)	8.20	6.15	4.10
m Si-P123 (g)	0.00	2.05	4.10

A certain amount of support was put in contact with the corresponding aqueous copper nitrate precursor solution. The metal precursor/silica composites were gently dried under air at 25 ± 1 °C for 5 days. The powders were sequentially submitted to calcination under stagnant air in a muffle oven at 500 °C for 6 h (heating ramp of 1.5 °C min^{-1}) to obtain the oxide forms of catalysts and burn off the organic components. To avoid the "container effect" throughout calcination,[33] the same open container and similar sample depths were used. After calcination, the solids were stored under ambient conditions in sealed flasks without special precautions. The samples were labeled as Cu_{10}/Mx.

Catalyst characterization

The thermogravimetric (TG) measurements were performed on a computer coupled Q-derivatograph (MOM). This analysis was performed for the supports to observe the difference between the loading degree with Si-P123 and were carried out in the temperature range between 20 and 600 °C with a heating rate of 10 °C min^{-1}. All measurements were performed under stagnant air.

Nitrogen physisorption measurements were carried out at −196 °C on an Autosorb MP-1 instrument from Quantachrome. Surface areas and pore volumes were calculated from the corresponding isotherms using conventional algorithms.

The SAXS and WAXS experiments were made on ID02 at 12.4 keV with d = 1.5m. The samples were inserted between two Kapton glasses. All measurements were dark subtracted and the background was measured with a double empty Kapton glass. All measurements were normalized by the transmission coefficient and by the acquisition time.

Diffuse reflectance UV-visible (DR UV-vis) spectra were recorded on a Shimadzu UV-2450 spectrometer equipped with an integrating sphere unit (ISR-2200). The spectra were collected in the range between 200–800 nm by using $BaSO_4$ as the reflectance standard.

Transmission Electron Microscopy (TEM) analyses were performed with a JEOL 1200 EXII.

Energy X-Ray dispersive spectroscopy (EDXS) analyses were performed with an environmental scanning electronic microscope Quanta 200 coupled with an Oxford INCA analyzer.

Temperature programmed reduction and chemisorption experiments were performed on a Chembet Pulsar TPR/TPD from Quantachrome. Amounts of about 30 mg of calcined sample were inserted in a U-shape microreactor. Before each TPR run, the catalyst was activated at 500 °C for 1 h under a flow of simulated air (40 mL min^{-1}). After cooling to 50 °C, the H_2 containing flow was stabilized (40 mL min^{-1}, 5 vol. % H_2 in Ar) and the TPR was performed from 50 to 500 °C with a temperature ramp of 5 °C min^{-1}.

The dispersion of metallic copper (D_{Cu}), average copper particle size (d_{Cu}) and active surface area (S_{Cu}) were determined using a nitrous oxide chemisorption method using specific algorithms.[34-37] The experiments were conducted on a Chembet Pulsar TPR/TPD from Quantachrome. The first reduction was carried out under the same conditions used for TPR, up to 350 °C. After the reduction step, the gas was switched to Ar and the reactor was cooled down to 50 °C, kept for 30 min, and then the gas was switched to N_2O (40 mL min^{-1}) for 30 min in order to oxidize the surface zero-valent Cu to Cu_2O. The sample was again flushed with pure Ar for 30 min, and then a second TPR run was performed.

Hydrogenation of trans-cinnamaldehyde

The liquid phase hydrogenation of cinnamaldehyde was carried out at *atmospheric pressure* in a round-bottom threeneck glass reactor equipped with a bubbler, magnetic stirrer and a reflux condenser. Prior to reaction all the samples were activated by reduction under flowing H_2 at 350 °C for 10 h with a heating ramp of 1.5 °C min^{-1}. The following reaction conditions were applied: 0.265 g of catalyst, 1.0 mL of trans-cinnamaldehyde, 25.0 mL of propylene carbonate as solvent, hydrogen flow of 1.0 L h^{-1}, reaction temperature of 150 °C, and agitation speed of 900 rpm.

Cu_{10}/M0-c and Cu_{10}/M50 samples were also tested at *high pressure*. The catalytic reaction was carried out in a Parr batch reactor under the following conditions: 0.265 g of catalyst, 1.0 mL of trans-cinnamaldehyde, 40 mL of 2-propanol as solvent, 10 bar of H_2, reaction temperature of 130 °C, and agitation speed of 750 rpm. At certain periods, aliquots of reaction mixture were withdrawn and analyzed with a gas-chromatograph (HP 5890 equipped with a DB-5 capillary column (25 m × 0.20 mm × 0.33 μm) and FID detector). The products were identified from the retention time of the pure compounds and also verified with a GC-MS (Agilent 6890N system equipped with an Agilent 5973 MSD detector and a DB-5-ms column). For the quantitative analyses, the FID response factors for each compound were taken into consideration. The selectivity towards the products and the total conversion were calculated as described in a previous paper.[38] For the recycling tests, Cu_{10}/M50 catalyst was recovered from the reaction mixture by centrifugation, washed with fresh 2-propanol and ethanol, dried, calcined and reactivated, before being tested under high-pressure conditions.

Results and discussion

Physico-chemical characterization

The TG analysis for the uncalcined supports (Figure 1) displayed three steps of weight loss. The first loss in weight corresponds to the removal of weakly adsorbed water

molecules, while the second weight loss relates to the water derived from the dehydroxilation of the surface sylanols and it is observed only for the M0 support between 130 and 180 °C.[39, 40] The third weight loss corresponds to the P123 decomposition and differs from one support to another.[41] For M25 it was detected from 180 °C, while for M50 it starts at 150 °C. Also M0 support shows the decomposition of the surfactant from 230 °C. The difference between the decomposition temperatures may came from the different loadings with Si-P123. High loadings conduct to lower decomposition temperatures suggesting that not all of the Si-P123 is integrated within the silica matrix. The supports show a final weight loss after the TG analysis up to 500 °C as follows: M0 – 11 wt. %, M25 – 17 wt. % and M50 – 25 wt. % in line with the gradual increase in the amount of surfactant bound on silica framework.

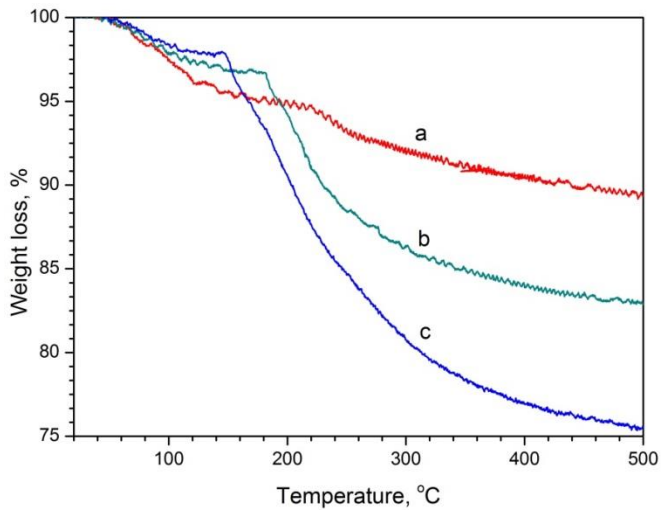

Figure 1. TG curves for the supports: a-M0, b-M25 and c-M50

Small angle X-ray scattering (SAXS) results for the calcined Cu-based materials are shown in Figure 2. All patterns display intense peaks accompanied by two less intense peaks, which were indexed as (100), (110) and (200) reflections which correspond to highly ordered hexagonal 2D materials with a *p6mm* symmetry.[42, 43] The results demonstrate the maintenance of pore symmetry of the parent supports and a good textural uniformity of these materials after impregnation and calcination. No significant shifts of the *q* values were observed along the series, indicating similar unit cell parameters of the obtained mesostructured composites, irrespective of the amount of Si-P123 used to prepare the functionalized supports. However, a clear variation in the intensity of peaks can be noticed. The most intense peaks were observed for Cu_{10}/M25 sample (Figure 2,b) suggesting the highest degree of mesostructure ordering together with a high dispersion of CuO NPs into the channels of the ordered mesoporous SBA-15-like silica.[44] The intensity peaks decreases for Cu_{10}/M0 sample (Figure 2, a), which can be tentatively interpreted by the increase in the extent of filling of the main mesopores with CuO NPs when compared with Cu_{10}/M25, taking also into account the TEM results showing oxide particles confined within the mesopores (*vide infra*). The sample Cu_{10}/M50 displays the lowest intensity of SAXS peaks indicative of a less ordered mesostructure at short- and long-range as compared with Cu_{10}/M0 and Cu_{10}/M25 samples, though the quality of the sample is high enough.

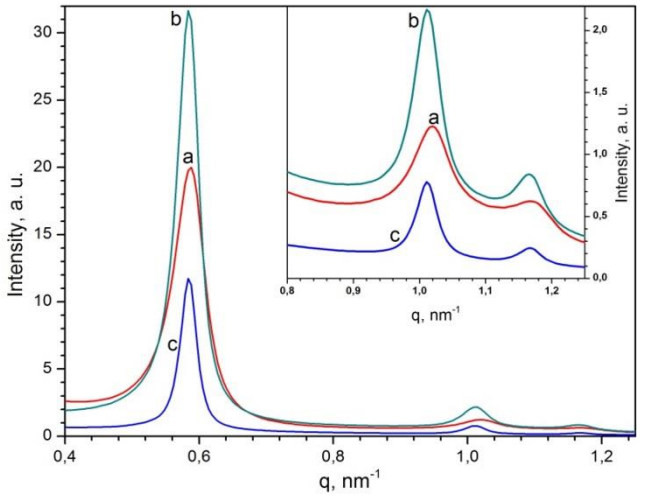

Figure 2. SAXS patterns for the oxide form of materials: a-Cu_{10}/M0, b-Cu_{10}/M25, c-Cu_{10}/M50

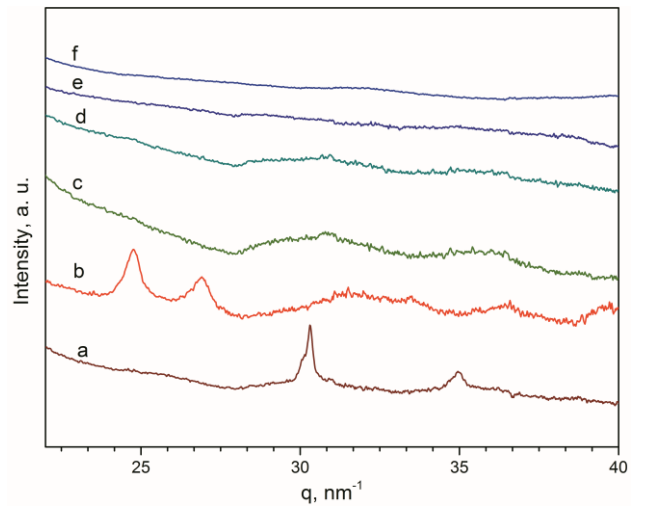

Figure 3. WAXS patterns for the oxide and metal forms of materials: a-Cu_{10}/M0(red), b-Cu_{10}/M0(calc), c-Cu_{10}/M25(red), d-Cu_{10}/M25(calc), e-Cu_{10}/M50(red), f-Cu_{10}/M50(calc)

Wide angle X-ray scattering (WAXS) was performed on the calcined (calc) and reduced (red) samples of Cu_{10}/M0, Cu_{10}/M25 and Cu_{10}/M50 (Figure 3). The WAXS patterns for Cu_{10}/M0, both oxide and metal forms, display small and broadened peaks attributed to CuO (Figure 3,b) and Cu^0 phases (Figure 3,a), respectively, indicating that the size of correspoding crystallites are small but detectable. In opposite, the samples Cu_{10}/M25 and Cu_{10}/M50 show hardly distinguishable diffraction peaks clearly indicating the presence

of only finely dispersed oxide and metallic crystallites with an average particle size below the detection limit of apparatus (less than ~3 nm).[45] This provides evidence that highly dispersed copper (oxide) nanoparticles suported on mesoporous silica at relatively high metal loading of 10 wt. % can be successfully synthesized *via* simple incipient wetness impregnation method by using polyether-functionalized mesoporous silica as supports. Likiwise, the results obviously show that the fabricated catalysts are resistant against particle sintering upon the calcination and reduction processes.

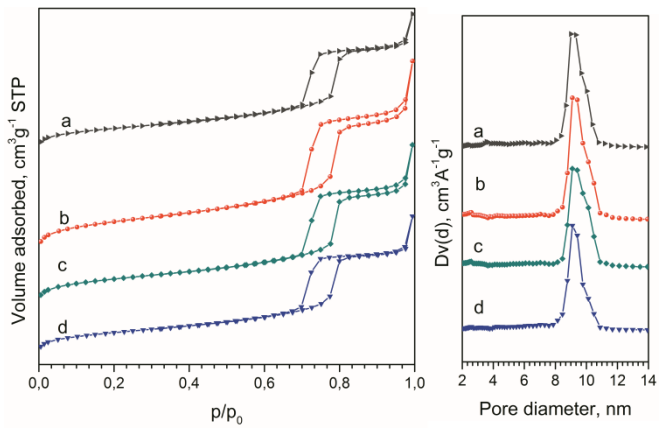

Figure 4. N_2 physisorption isotherms for the oxide form of materials (left) and NL-DFT pore size distribution (right) for the oxide forms of materials: a-Cu_{10}/M0-c, b-Cu_{10}/M0, c-Cu_{10}/M25, d-Cu_{10}/M50

The textural characteristics of the functionalized supports and oxide-loaded samples were evaluated from the nitrogen adsorption-desorption isotherms. Figure 4 displays the isotherms and the pore size distributions for the oxide form of catalysts, whereas Table 2 centralizes the textural properties of both supports and catalysts. Characteristic IUPAC type IV isotherms alongside H1 hysteresis loops can be noticed for all samples. Also, from NL-DFT pore size distribution, a narrow distribution of the pores was observed according to their diameter. These features point towards ordered SBA-15-like mesostructures having narrow size distributions of the cylindrical mesopores, and indicate that the mesoporous structure of the supports was retained after the deposition of copper oxide,[46] which is in good agreement with the SAXS analysis. It is worthy of note that the hysteresis loops show no forced closures on the desorption branches of the isotherms, suggesting the absence of cavitation effects resulting from the partial blockage of primary mesopores with metal oxide NPs, which usually occurs when particles are mainly confined whitin the mesopores of the support.[4]

Data displayed in Table 2 illustrate the net effect of Si-P123 content on the textural properties of supports. Thus, uncalcined M0 support prepared without Si-P123 shows the highest specific surface area along the series (996 m^2 g^{-1}). With the gradual increase in the amount of bis-silylated surfactant the specific area slightly decreases to 917 m^2 g^{-1} for M25 and then significantly decreases to 646 m^2 g^{-1} for M50, in line with the presence of more surfactant covalently bound to silica framework, occluding thus the mesopores and the micropores of support. This may explain the significant drop of microporous area from 266 to 98 and 25 m^2 g^{-1} as the amount of Si-P123 increases from 0 to 25 and 50 wt. %, respectively. At the same time, the pore volume and pore size are similar for M0 and M25 supports (around 1.8 cm^3 g^{-1} and 9.7 nm) and they decrease for M50 sample (1.43 cm^3 g^{-1} and 9.2 nm). On the other side, all the textural properties decline when M0 support is subjected to calcination due to the dehydroxylation of the silica surface and shrinkage of the mesostructure. For example, the specific surface area decreases from 996 to 719 m^2 g^{-1} whereas the pore diameter decreases from 9.7 to 9.3 nm.

All the oxide-loaded mesoporous silicas show lower specific areas than the parent uncalcined supports due to the thermal treatment upon calcination and as a result of loading the pores with phases of copper oxide. It is interesting to observe that after calcination, the microporous surface area of Cu_{10}/M25 and Cu_{10}/M50 increases as compared with the parent supports (for example from 25 to 113 m^2 g^{-1} for M50), which can be associated with the removal of the micropore-occluded surfactant. The pore diameter for all oxide forms of materials was found to be in a small range from 9.1 to 9.3 nm.

Table 2. Textural properties for M0-c, M0, M25, and M50 supports and oxide form of materials

Sample	S_{BET} (m^2 g^{-1})	S_μ (m^2 g^{-1})	V_p (cm^3 g^{-1})	V_μ ($cm^3 g^{-1}$)	D_p (nm)
M0-c	719	173	1.25	0.080	9.3
Cu_{10}/M0-c	582	116	1.07	0.051	9.3
M0	996	266	1.74	0.127	9.7
Cu_{10}/M0	855	244	0.97	0.116	9.3
M25	917	98	1.84	0.036	9.7
Cu_{10}/M25	684	174	0.98	0.081	9.2
M50	646	25	1.43	0.001	9.2
Cu_{10}/M50	590	113	0.98	0.051	9.1

S_{BET} – specific surface area, Sμ – micropore surface area, V_p – pore volume, V_μ – micropore volume, D_p – pore diameter

Transmission electron microscopy (TEM) images recorded at low-resolution was performed for both oxide-loaded samples and the reduced catalysts (Figure 5). As a first remark, all the solids display hexagonal mesoporous structure with a high long-range order and narrow pore size distribution, typical for SBA-15-like materials, confirming SAXS and N_2 physisorption results. The silica grains appeared free from large aggregates on the external surface even after the reduction process, confirming thus WAXS data. In the case of Cu_{10}/M0 (calc) and Cu_{10}/M0 (red) small copper particles were observed confined inside the silica channels, though some particles appearing larger than the pore diameter can be also observed. However,

Cu_{10}/M25 materials display no distinguishable particles, even after the reduction process, clearly indicating that the particles are indeed highly dispersed. The TEM images recorded on Cu_{10}/M50 samples are qualitatively very similar to those of Cu_{10}/M25 and for the sake of brevity are not shown here. Anyway, the TEM results are in excellent agreement with the corresponding WAXS analyses.

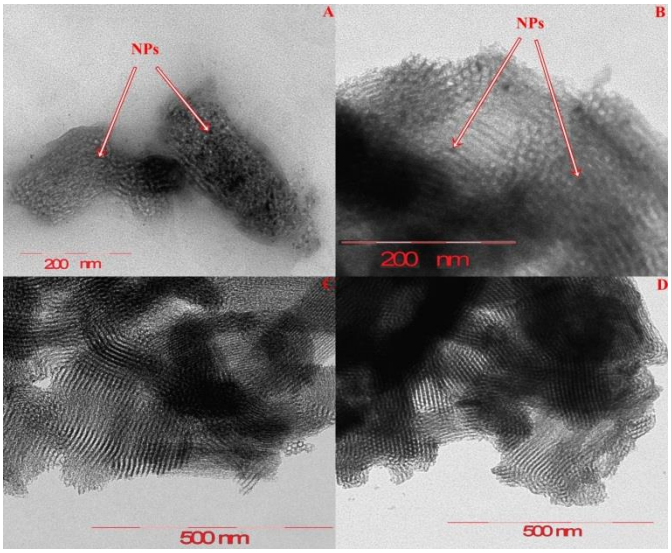

Figure 5. TEM images for (A) Cu10/M0 (calc), (B) Cu10/M0 (red), (C) Cu10/M25 (calc) and (D) Cu10/M25 (red)

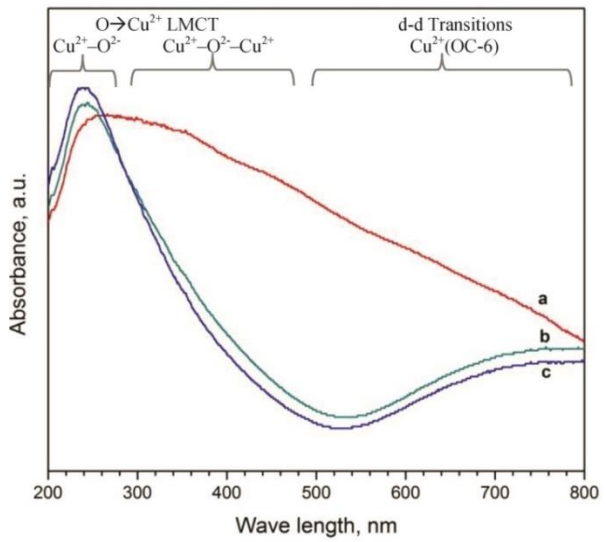

Figure 6. DR UV-Vis spectra for the oxide form of materials: a-Cu_{10}/M0, b-Cu_{10}/M25, c-Cu_{10}/M50

Cu_{10}/M0, Cu_{10}/M25 and Cu_{10}/M50 in their oxidized forms were also investigated by diffused reflectance UV-Vis spectroscopy. All the recorded spectra (Figure 6) display a absorption maximum between 230 – 270 nm which can be assigned to charge transfer of the type Ligand-to-Metal Charge Transfer (LMCT) which is characteristic of highly dispersed copper (isolated) Cu^{2+}-O^{2-} in octahedral coordination environment.[47] The Cu_{10}/M0 (a) displays a continuous absorption in the 300 – 650 nm range which can be related to the presence of linear oligonuclear Cu^{2+} clusters (for example, species like (Cu-O-Cu)$^{2+}$).[48] The maximum observed for Cu_{10}/M25 (b) and Cu_{10}/M50 (c) located between 600 and 800 nm, seen also in Cu_{10}/M0 curve, was assigned to the d–d transition band of the Cu^{2+} ions into a pseudo-octahedral environment or charge-transfer transitions from other lower-symmetry Cu species (e.g., square planar CuO_x, 1D Cu chains).[47, 49, 50] The spectroscopy results represent therefore a confirmation on the presence of highly dispersed CuO clusters of low nuclearity for Cu_{10}/M25 and Cu_{10}/M50 materials and of larger CuO particles for Cu_{10}/M0.

The reducibility of the oxide-loaded materials was analysed *via* TPR and the registered curves are illustrated in Figure 7. First of all, the experimental hydrogen consumption was close to that theoretically calculated taking into account the elemental analysis of the calcined samples, and therefore the TPR profiles reflect the total reduction of CuO to zero-valent metallic copper. As stated in literature, the reduction temperature of copper oxide depends on the particle size and also on the dispersion, lower temperatures being associated with higher dispersions.[51,52] The profiles for Cu_{10}/M0, Cu_{10}/M25 and Cu_{10}/M50 (curves b, c and d) display reduction maxima in a narrow temperature range of 250-260 °C, signifying the reduction of copper cations in highly dispersed CuO particles. In contrast, the TPR profile of Cu_{10}/M0-c shows a maximum of reduction temperature shifted at ~275 °C, suggesting the lowest dispersion of CuO along the series.

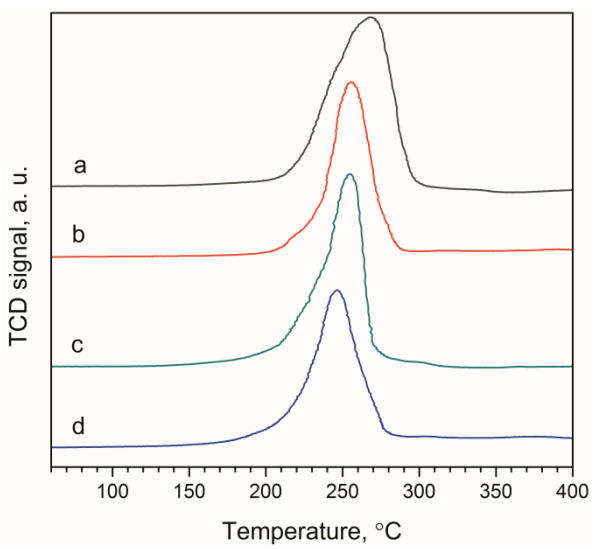

Figure 7. TPR profiles of oxide forms of materials: a-Cu_{10}/M0-c, b-Cu_{10}/M0, c-Cu_{10}/M25, d-Cu_{10}/M50

The results presented so far highlight the positive role of polyether chains in stabilizing Cu^{2+} ions upon impregnation, most likely by coordination with oxygen atoms in the

hydrophillic ethylene oxide –CH_2-O-CH_2- groups of polyetheric surfactants. A similar stabilizing mechanism in the case of CuO/SBA-15 materials was recently proposed by Chen et al.[14] involving the coordination of Cu^{2+} ions with carboxylate COO^- groups. By controlling the content of the functionalized surfactant in synthesis gel, novel organic-inorganic SBA-15-like hybrids containing occluded P123 triblock polymer covalently bound to the silica framework can be designed, creating unique hydrophilic microenvironments between the silica wall and template aggregates, which can be further exploited as confined spaces to directly infiltrate hydrophilic metal precursor species for a rapid functionalization. Upon surfactant removal by calcination, decomposition of copper precursors to stabilized copper oxide takes place, resulting in intra-porous copper species highly dispersed on the surface of the SBA-15-like materials. On the other hand, taking into account that another type of interaction may occur between copper precursors with silica walls through Si-OH silanol groups to stabilize the oxide phases, the density of these groups may play also a crucial role. Indeed, our results show that as compared with the uncalcined M0 support, which presumably has high density of silanol groups (the surfactant was removed by extraction with ethanol), the use of calcined M0 as support conducted to poorly dispersed CuO (and Cu^0) particles (*vide infra*) because of the dehydroxylation of silanols resulting in less stabilizing surface groups, and favouring thus serious CuO aggregation. Indeed, previous studies suggested that a high copper dispersion on SBA-15 mesoporous silica is facilitated when the surface is rich in silanol groups.[43, 53] For example, Wang et al. showed that abundant silanol groups in as-prepared SBA-15 silica favors the enhancement of host–guest interactions, leading to a higher dispersion level of the guest copper species, when compared with calcined SBA-15.[53]

To evaluate copper dispersion, the titration of superficial copper atoms with N_2O was performed. Table 3 illustrates the metal loading degrees, dispersion degrees, Cu surface areas, and Cu average particle sizes for all catalysts. EDXS analysis confirms the loading degree, which is close to the calculated ones within experimental errors (10 wt. %). As expected, Cu_{10}/M50 has the highest surface area (389 m^2_{Cu} g^{-1}_{Cu}) and decreases for Cu_{10}/M25 (322 m^2_{Cu} g^{-1}_{Cu}) and further for Cu_{10}/M0 (296 m^2_{Cu} g^{-1}_{Cu}), thus confirming the positive effect of the bis-silylated surfactant used. The dispersion degree and the average Cu particle size follow the same pattern as Cu surface area, for Cu_{10}/M50 high dispersion (57,5 %) conducts to a low particle size (1,7 nm), also for Cu_{10}/M25 decreasing with 10 % the dispersion leads to higher particle size (2,1 nm). The catalysts prepared without using Si-P123 displays a dispersion degree of 43,7 % and 2,3 nm particle size, the lowest dispersion and the highest particle size among the samples prepared with uncalcined (extracted) supports. However, if the support is subjected to calcination prior impregnation, the dispersion degree falls with a factor of five to 8,3 %, while the average particle size increases with a factor of 6 (12 nm), conducting to a low Cu surface area (56,1 m^2_{Cu} g^{-1}_{Cu}). It is finally worthy to note that as compared with relevant literature data obtained over copper-based mesoporous materials, our catalysts show very high dispersions and high surface areas of catalytic active sites. For instance, at similar copper loading (10.9 *vs* 10.6 %), Cu_{10}/M50 displays a much higher dispersion than Cu_{10}/SBA-15 prepared over mesoporous SBA-15 functionalized with –COOH groups (57.5 *vs* 37 %) in line with the higher copper surface area (42.4 *vs* 25 m^2_{Cu} g^{-1}_{cat}).[13] Such a comparison is particularly interesting to emphasize the effectiveness of our approach to fabricate by a simple method highly dispersed and stable nanosized copper nanoparticles supported on mesoporous host structures.

Table 3. EDXS and N_2O chemisorption data for copper catalysts

Sample	EDXS Cu (wt. %)	N_2O chemisorption			
		D_{Cu} (%)	d_{Cu} (nm)	S_{Cu} (m^2_{Cu} g^{-1}_{Cu})	S_{Cu} (m^2_{Cu} g^{-1}_{cat})
Cu10/M0-c	9.9	8.3	12.0	56	5.6
Cu10/M0	10.0	43.7	2.3	296	29.6
Cu10/M25	11.4	47.7	2.1	322	36.8
Cu10/M50	10.9	57.5	1.7	389	42.4

D_{Cu} - dispersion degree, d_{Cu} – average size of Cu particles, S_{Cu} – Cu surface area

Catalytic performance in hydrogenation of cinnamaldehyde

The catalytic performance of synthesized materials was evaluated in the liquid phase hydrogenation of cinnamaldehyde (CNA) with the purpose of investigating the activity and selectivity in relation with the physico-chemical properties of the samples. As seen in Scheme 1, the hydrogenation proceeds in two major directions, the hydrogenation of C=C and C=O double bonds, with the formation of hydrocinnamaldehyde (HCNA) and cinnamyl alcohol (CNOL), respectively. These two main compounds can be totally hydrogenated leading to the formation of hydrocinnamyl alcohol (HCNOL).

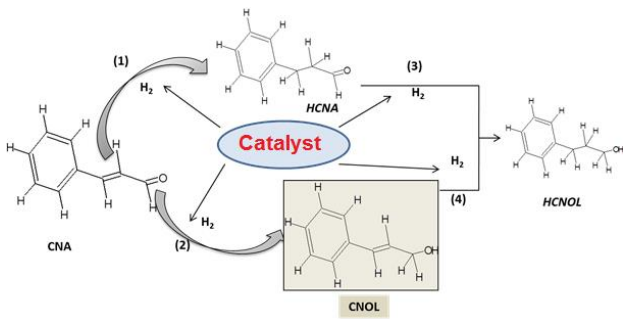

Scheme 1. Reaction pathways for the hydrogenation of cinnamaldehyde

The progression of CNA conversion *vs* time under atmospheric pressure (Patm) as well as 10 bar (P10) is illustrated in Figure 8. It can be observed that all catalysts derived from uncalcined (extracted) supports are highly active in hydrogenation, being able to completely convert the substrate in a maximum of 300 min of reaction. In opposite, the catalyst obtained on a calcined

M0 support manifested a very low catalytic activity (conversion of ~3 mol % in 360 min of reaction). The results are very interesting considering the mild reaction conditions, especially the atmospheric pressure. Under these conditions, the catalytic activity follows the order: Cu_{10}/M0-c << Cu_{10}/M0 < Cu_{10}/M25 < Cu_{10}/M50, in fair agreement with the evolution of S_{Cu} (m^2 g^{-1}_{cat}) (see Table 3). Indeed, Cu_{10}/M0-c showed a negligible catalytic activity due to the low capacity of poorly dispersed copper to activate the hydrogen molecules. However, examples from literature show that in order to have enhanced chemisorption capacity and hence superior intrinsic activity in the hydrogenation of CNA, the number of low-coordinated Cu^0 sites must be high, which can be achieved only for highly dispersed copper nanoparticles.[38, 54-56]

Further improvement in the catalytic activity was made by increasing the hydrogen pressure. Thus, two samples with extreme catalytic activity were tested under 10 bar H_2, Cu_{10}/M0-c and Cu_{10}/M50, respectively. As expected, increasing the pressure from atmospheric pressure to 10 bar concludes to an enhanced catalytic activity, from 240 min of total conversion to 45 min of total conversion for Cu_{10}/M50 and from 3 mol % after 360 min to ~ 30 mol % after the same period for Cu_{10}/M0-c.

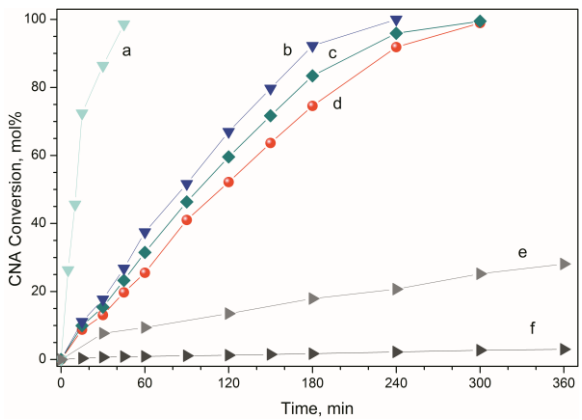

Figure 8. Catalytic activity of copper catalysts: a-Cu_{10}/M50-P10, b-Cu_{10}/M50-Patm, c-Cu_{10}/M25-Patm, d-Cu_{10}/M0-Patm, e-Cu_{10}/M0-calc-P10 and f-Cu_{10}/M0-c-Patm

The selectivities achieved for all tested samples are displayed in Table 4, as calculated at a CNA isoconversion of 30 mol %. Exception shows Cu_{10}/M0-c-Patm (run 1), for which the selectivity was not calculated due to the low conversion level. It can be observed that at atmospheric pressure, high selectivities towards saturated aldehyde HCNA (> 70 %) are obtained (runs 3-5). With the increase in the hydrogen pressure to 10 atm, the selectivities are still towards HCNA, but with a slight increase in the selectivity towards unsaturated alcohol CNOL from 17 to 23 mol % for Cu10/M50 catalyst (run 5 *vs* run 6), as also reported in other studies dealing with the effect of hydrogen pressure on the catalytic performances of the supported metals in the hydrogenation of α,β – unsaturated aldehydes.[57, 58]

It can be concluded that irrespective of pressure, finely dispersed metallic copper NPs on mesoporous silica manifest outstanding catalytic activity in hydrogenation but low selectivity towards CNOL, this is in agreement with other studies on copper-based catalysts. In addition, analysis of our data as compared with literature highlights that copper supported on functionalized ordered mesoporous silica developed in this study are among the most active copper based catalysts, under similar reaction conditions of temperature and pressure. For instance, in 2011 Volpe et al. obtained a conversion of ~40 mol % on a Cu/MCM-48 (2,5 wt. % Cu) sample after 300 min when the reaction was conducted at 10 atm.[30] Also in 2012, the same team proved a decrease in conversion to ~25 mol % after 220 min with another Cu/MCM-48 (4,1 wt. % Cu).[31] Marchi et al.[54] with a Cu/SiO_2 (8,1 wt. %) after 480 min arrived to a conversion of cinnamaldehyde of 58 mol % also in high pressure reaction conditions. In comparison, our catalysts completely converted the cinnamaldehyde after 300 min where the reaction was conducted under atmospheric pressure. Increasing the pressure of the reaction (10 bar), total conversion is achieved after 45 min. To carry out a straightforward comparison with the results from literature, the activity of Cu_{10}/M50 was also calculated under the form of turnover frequency (TOF, in moles of CNA converted per mole of surface copper per unit time). A TOF value of $23 \cdot 10^{-3}$ s^{-1} was obtained under 10 bar H_2, which was much higher than those values previously reported for Cu/MCM-48 ($1 \cdot 10^{-3}$ s^{-1}), Cu/MCM-41 ($2 \cdot 10^{-3}$ s^{-1}), Cu/CeO_2 ($7.4 \cdot 10^{-3}$ s^{-1}), and even for unsupported Cu NPs ($8 \cdot 10^{-3}$ s^{-1}).[8] Furthermore, under atmospheric pressure, Cu_{10}/M50 demonstrated a high TOF value of $3 \cdot 10^{-3}$ s^{-1}, thus confirming the oustanding activity of our catalysts.

Table 4. Selectivities for all the tested samples at 30 mol % isoconversion

Run	Sample	Selectivity (mol %)		
		HCNA	CNOL	HCNOL
1	Cu10/M0-c-Patm	-	-	-
2	Cu10/M0-c-P10	54	43	3
3	Cu10/M0-Patm	82	12	6
4	Cu10/M25-Patm	77	13	10
5	Cu10/M50-Patm	73	17	10
6	Cu10/M50-P10	62	23	15

Patm - reaction was conducted at atmospheric pressure

P10 – reaction was conducted at 10 atm hydrogen pressure

In order to further enhance chemoselectivity of catalysts towards unsaturated alcohol, the metal form of Cu_{10}/M50 catalyst was subjected to an oxidation treatment for 5 min with synthetic air at 300 °C.[59] A TPR curve was registered before and after the oxidation treatment. The corresponding profiles are displayed in Figure 9, noticing that the curve (a) is very similar to that reported in Figure 7,d. It is clear that the oxidized sample shows a different reduction behaviour, characterized by an important peak with maximum at around 185 °C. This can be explained by the fact that a part of surface Cu^0 was oxidized to Cu_2O upon the applied treatment.[60] Therefore, this low-temperature peak is attributed to the reduction of Cu^+ to Cu^0, in agreement with previous studies.[61, 62]

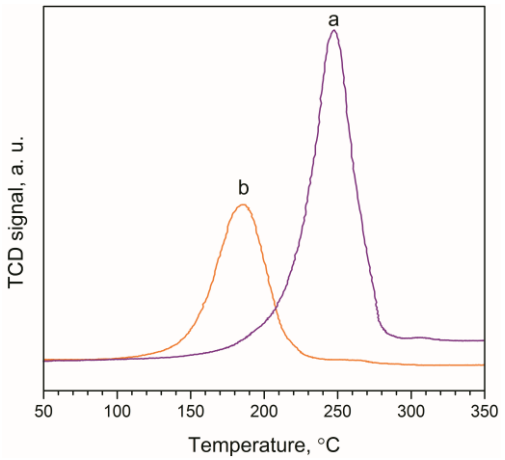

Figure 9. TPR profiles for Cu_{10}/M50 catalysts: a- before oxidation, b- after oxidation.

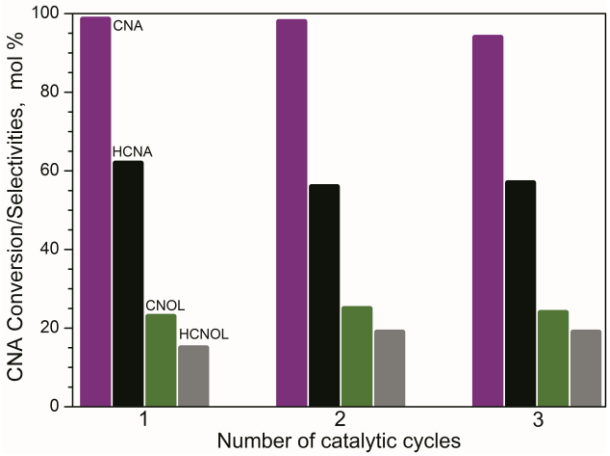

Figure 11. Recycling tests for Cu_{10}/M50 catalyst (CNA conversion after 45 min of reaction; selectivities at 30 mol % isoconversion)

The catalytic performance of the material prepared is this way was compared with that of Cu_{10}/M50 catalyst without the oxidation treatment. The catalytic results obtained under atmospheric pressure are displayed in Figure 10 for Cu_{10}/M50 without oxidation (A) and after oxidation treatment (B). It can be observed that the selectivity profiles are totally different. The original catalyst shows selectivity towards HCNA higher than 60 mol % at all conversion levels, whereas the selectivity to CNOL is the utmost of ~30 mol % at low conversion levels (~ 20 mol %) and continuously decreases to null with the increase in the conversion. In contrast, the oxidized Cu_{10}/M50 catalyst shows higher selectivity to CNOL of ~ 60 mol % at ~ 50 mol % conversion, yet the reaction rate is strongly diminished (conversion of ~ 50 mol % after 1600 min of reaction). These interesting results can be easily rationalized by considering that upon oxidative treatment, Cu_2O decorating metallic Cu^0 NPs is obtained, generating cooperative metal-electron deficient sites (Cu^0/Cu^+) that could activate the molecular hydrogen (Cu^0) and carbonyl group of unsaturated aldehyde (Cu^+), respectively and improve chemoselectivity, at the expense of decreasing activity owing to the reduction of the number of metal active sites.[63-66]

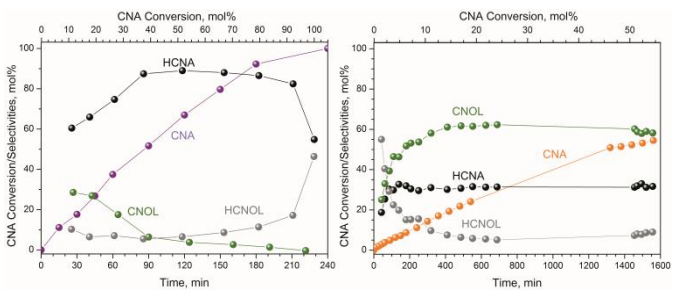

Figure 10. Catalytic activity and selectivity profiles for Cu_{10}/M50 catalysts: A- before oxidation, B- after oxidation for 5 min. Selectivity is plotted *vs* conversion.

Finnaly, the reusability of Cu_{10}/M50 material was evaluated upon three catalytic runs. An essentially constant chemoselectivity and a slight decrease in activity were observed after the 3rd run (Figure 11), in line with the minor decrease in the dispersion degree of copper measured for the corresponding spent catalyst, as compared with the fresh sample (56.1 *vs* 57.5 %). These results demonstrate the possibility to reuse the spent catalysts as well as the good stability of copper nanoparticles synthesized on polyether-functionalized ordered mesoporous silica after repeating calcination-reduction cycles.

Conclusions

Polyether-functionalized SBA-15-like mesoporous materials were successfully used as host structures to prepare highly dispersed copper nanoparticles below 2 nm in size, at high metal loading of 10 wt. %, with outstanding dispersion degrees of up to 57.5 %. A strong dependence of the amount of Si-P123 used for the support synthesis on the morpho-structural properties of materials was demonstrated by various techniques. Increasing the amount of functionalized surfactant up to 50 wt. % leads to an increase in copper active surface area, a decrease in the average particle, in line with enhanced dispersion degrees. The copper supported catalysts manifest excellent activity in the cinnamaldehyde hydrogenation reaction and high selectivity towards saturated aldehyde (>70 mol %), under atmospheric pressure conditions. However, improvement in both activity and selectivity towards the unsaturated alcohol (~ 60 mol %) was attained by increasing the hydrogen pressure and by applying a two-step reduction-oxidation pre-treatment, to obtain cooperative metal-electron deficient Cu^0/Cu^+ sites. In addition, the catalysts were reusable, with no significant changes in catalytic performance and the degree of copper dispersion after three catalytic runs.

Acknowledgements

This work was partially supported by two grants of the Romanian National Authority for Scientific Research, CNCS-UEFISCDI (project numbers PN-II-RU-TE-2012-3-0403 and PN-II-ID-PCE-2011-3-0868).

Notes and references

[a]"Gheorghe Asachi" Technical University of Iasi, Faculty of Chemical Engineering and Environmental Protection, Laboratory of Catalysis, 73 Prof. Dr. docent Dimitrie Mangeron Street, 700050 Iasi, Romania. Tel: +40 - 232 278683;
*E-mail: aungureanu@tuiasi.ro
[b]Institut Charles Gerhardt Montpellier, UMR 5253, Chimie Moleculaire et Organisation du Solide, cc 1701, Universite Montpellier, Place E. Bataillon, 34095 Montpellier Cedex 5 France. Tel. +33-(0)4-67-14-38-32;
*E-mail: ahmad.mehdi@univ-montp2

1. J. M. Campelo, D. Luna, R. Luque, J. M. Marinas, A. A. Romero, *ChemSusChem*, 2009, **2**, 18-45.
2. B. R. Cuenya, *Thin Solid Films*, 2010, **518**, 3127-3150.
3. P. Mäki-Arvela, J. Hájek, T. Salmi, D. Y. Murzin, *Appl Catal A-Gen*, 2005, **292**, 1-49.
4. A. Ungureanu, B. Dragoi, A. Chirieac, C. Ciotonea, S. Royer, D. Duprez, A. S. Mamede, E. Dumitriu, *Acs Appl Mater Inter*, 2013, **5**, 3010-3025.
5. B. Dragoi, A. Ungureanu, A. Chirieac, V. Hulea, S. Royer, E. Dumitriu, *Catal Sci Tech*, 2013, **3**, 2319-2329.
6. T. Ressler, B. L. Kniep, I. Kasatkin, R. Schlogl, *Angew Chem Int Ed Engl*, 2005, **44**, 4704-4707.
7. G. Prieto, J. Zečević, H. Friedrich, K. P. de Jong, P. E. de Jongh, *Nat Mater*, 2013, **12**, 34-39.
8. V. Gutiérrez, F. Nador, G. Radivoy, M. A. Volpe, *Appl Catal A-Gen*, 2013, **464-465**, 109-115.
9. P. Munnik, M. Wolters, A. Gabrielsson, S. D. Pollington, G. Headdock, J. H. Bitter, P. E. de Jongh, K. P. de Jong, *J Phys Chem C*, 2011, **115**, 14698-14706.
10. K. Yoshida, C. Gonzalez-Arellano, R. Luque, P. L. Gai, *Appl Catal A-Gen*, 2010, **379**, 38-44.
11. S. Wang, W. Guo, H. Wang, L. Zhu, S. Yin, K. Qiu, *New J Chem*, 2014, **38**, 2792.
12. C. Ciotonea, B. Dragoi, A. Ungureanu, A. Chirieac, S. Petit, S. Royer, E. Dumitriu, *Chem Commun*, 2013, **49**, 7665-7667.
13. C.-S. Chen, C.-C. Chen, C.-T. Chen, H.-M. Kao, *Chem Commun*, 2011, **47**, 2288-2290.
14. C. S. Chen, Y. T. Lai, T. W. Lai, J. H. Wu, C. H. Chen, J. F. Lee, H. M. Kao, *ACS Catal*, 2013, **3**, 667-677.
15. J. Gu, Y. Huang, S. P. Elangovan, Y. Li, W. Zhao, I. Toshio, Y. Yamazaki, J. Shi, *J Phys Chem C*, 2011, **115**, 21211-21217.
16. A. F. Grandsire, C. Laborde, F. Lamaty, A. Mehdi, *Appl Organomet Chem*, 2010, **24**, 179-183.
17. Y. Yuan, S. Yao, M. Wang, S. Lou, N. Yan, *Curr Org Chem*, 2013, **17**, 400-413.
18. M. Chatterjee, F. Zhao, Y. Ikushima, *Appl Catal A-Gen*, 2004, **262**, 93-100.
19. A. Jung, A. Jess, T. Schubert, W. Schutz, *Appl Catal a-Gen*, 2009, **362**, 95-105.
20. Y. Li, C. H. Ge, J. Zhao, R. X. Zhou, *Catal Lett*, 2008, **126**, 280-285.
21. P. N. Rylander, in *Catalytic Hydrogenation Over Platinum Metals*, eds. P. N. Rylander, Academic Press, 1967, pp. 238.
22. D. Richard, P. Gallezot, D. Neibecker, I. Tkatchenko, *Catal. Today*, 1989, **6**, 171-179.
23. P. V. Samant, M. F. R. Pereira, J. L. Figueiredo, *Catal Today*, 2005, **102**, 183-188.
24. A. Giroir-Fendler, D. Richard, P. Gallezot, in *Studies in Surface Science and Catalysis*, eds. J. B. C. B. D. D. C. M. M. Guisnet and G. Pérot, Elsevier, 1988, vol. 41, pp. 171.
25. F. López-Linares, M. G. Gonzalez, D. E. Páez, *J Mol Catal A: Chem*, 1999, **145**, 61-68.
26. J. Hájek, N. Kumar, P. Mäki-Arvela, T. Salmi, D. Y. Murzin, I. Paseka, T. Heikkilä, E. Laine, P. Laukkanen, J. Väyrynen, *Appl Catal A-Gen*, 2003, **251**, 385-396.
27. H. L. Liu, M. L. Yuan, C. H. Guo, R. X. Li, H. Y. Fu, H. Chen, X. J. Li, *Chinese J Catal*, 2011, **32**, 1256-1261.
28. M. L. Toebes, F. F. Prinsloo, J. H. Bitter, A. J. van Dillen, K. P. de Jong, *J Catal*, 2003, **214**, 78-87.
29. P. Reyes, C. Rodriguez, G. Pecchi, J. L. G. Fierro, *Catal Lett*, 2000, **69**, 27-32.
30. V. S. Gutiérrez, A. S. Diez, M. Dennehy, M. A. Volpe, *Micropor Mesopor Mat*, 2011, **141**, 207-213.
31. V. Gutierrez, M. Alvarez, M. A. Volpe, *Appl Catal A-Gen*, 2012, **413-414**, 358-365.
32. C. J. Brinker and G. W. Scherer, *Sol-Gel Science: The Physics and Chemistry of Sol-Gel Processing*, *1st ed.*, Academic Press, 1990, pp. 140-142.
33. X. Sun, Y. Shi, P. Zhang, C. Zheng, X. Zheng, F. Zhang, Y. Zhang, N. Guan, D. Zhao, G. D. Stucky, *J Am Chem Soc*, 2011, **133**, 14542-14545.
34. G. C. Chinchen, C. M. Hay, H. D. Vandervell, K. C. Waugh, *J Catal*, 1987, **103**, 79-86.
35. K.-W. Jun, W.-J. Shen, K. S. Rama Rao, K.-W. Lee, *Appl Catal A-Gen*, 1998, **174**, 231-238.
36. J. W. Evans, M. S. Wainwright, A. J. Bridgewater, D. J. Young, *Appl Catal*, 1983, **7**, 75-83.
37. G. Krishna Reddy, K. S. Rama Rao, P. Kanta Rao, *Catal Lett*, 1999, **59**, 157-160.
38. B. Dragoi, A. Ungureanu, A. Chirieac, V. Hulea, E. Dumitriu, *Acta Chim Slov*, 2010, **57**, 677-685.
39. D. Zhao, J. Feng, Q. Huo, N. Melosh, G. H. Fredrickson, B. F. Chmelka, G. D. Stucky, *Science*, 1998, **279**, 548-552.
40. D. Zhao, Q. Huo, J. Feng, B. F. Chmelka, G. D. Stucky, *J Am Chem Soc*, 1998, **120**, 6024-6036.
41. M. Kruk, M. Jaroniec, C. H. Ko, R. Ryoo, *Chem Mater*, 2000, **12**, 1961-1968.
42. B. Samran, T. J. White, S. Wongkasemjit, *J Porous Mater*, 2010, **18**, 167-175.
43. N. Brodie-Linder, R. Besse, F. Audonnet, S. LeCaer, J. Deschamps, M. Impéror-Clerc, C. Alba-Simionesco, *Micropor Mesopor Mat*, 2010, **132**, 518-525.
44. J. D. F. Ramsay, S. Kallus, E. Hoinkis, in *Studies in Surface Science and Catalysis*, eds. G. K. K.K. Unger, J. P. Baselt, Elsevier, Heidelburg, Germany, 2000, vol. 128, p. 439.
45. W. Wei, Y. Lu, W. Chen, S. Chen, *J Am Chem Soc*, 2011, **133**, 2060-2063.

46. C. P. Jaroniec, M. Kruk, M. Jaroniec, A. Sayari, *J Phys Chem B*, 1998, **102**, 5503-5510.
47. J. J. Bravo-Suárez, B. Subramaniam, R. V. Chaudhari, *J Phys Chem C*, 2012, **116**, 18207-18221.
48. M. Ramakrishna Prasad, G. Kamalakar, S. J. Kulkarni, K. V. Raghavan, *J Mol Catal A: Chem*, 2002, **180**, 109-123.
49. M. Shimokawabe, N. Takezawa, H. Kobayashi, *Appl Catal*, 1982, **2**, 379-387.
50. M. Arai, S. Nishiyama, S. Tsuruya, M. Masai, *J Chem Soc, Faraday Trans*, 1996, **92**, 2631-2636.
51. X.-C. Zheng, S.-H. Wu, S.-P. Wang, S.-R. Wang, S.-M. Zhang, W.-P. Huang, *Appl Catal A-Gen*, 2005, **283**, 217-223.
52. C.-H. Tu, A.-Q. Wang, M.-Y. Zheng, X.-D. Wang, T. Zhang, *Appl Catal A-Gen*, 2006, **297**, 40-47.
53. Y. M. Wang, Z. Y. Wu, H. J. Wang, J. H. Zhu, *Adv Funct Mater*, 2006, **16**, 2374-2386.
54. A. J. Marchi, D. A. Gordo, A. F. Trasarti, C. R. Apesteguía, *Appl Catal A-Gen*, 2003, **249**, 53-67.
55. S. Valange, A. Derouault, S. Pronier, J. Barrault, Z. Gabelica, in *Studies in Surface Science and Catalysis*, eds. N. Ž. J. Čejka and P. Nachtigall, Elsevier, 2005, vol. 158, Part B, p. 1557.
56. Z. Liu, Y. Yang, J. Mi, X. Tan, Y. Song, *Catal Commun*, 2012, **21**, 58-62.
57. Y. Sun, R. N. Landau, J. Wang, C. LeBlond, D. G. Blackmond, *J Am Chem Soc*, 1996, **118**, 1348-1353.
58. G. Papp, J. Elek, L. Nadasdi, G. Laurenczy, F. Joo, *Adv Synth Catal*, 2003, **345**, 172-174.
59. J. Rodriguez, J. Kim, J. Hanson, M. Pérez, A. Frenkel, *Catal Lett*, 2003, **85**, 247-254.
60. C.-S. Chen, W.-H. Cheng, S.-S. Lin, *Catal Lett*, 2000, **68**, 45-48.
61. C. J. G. Van Der Grift, A. F. H. Wielers, B. P. J. Jogh, J. Van Beunum, M. De Boer, M. Versluijs-Helder, J. W. Geus, *J Catal*, 1991, **131**, 178-189.
62. A. Gervasini, S. Bennici, *Appl Catal A-Gen*, 2005, **281**, 199-205.
63. A. Chambers, S. D. Jackson, D. Stirling, G. Webb, *J Catal*, 1997, **168**, 301-314.
64. S. Valange, A. Derouault, J. Barrault, Z. Gabelica, *J Mol Catal A: Chem*, 2005, **228**, 255-266.
65. G. J. Hutchings, F. King, I. P. Okoye, M. B. Padley, C. H. Rochester, *J Catal*, 1994, **148**, 453-463.
66. G. J. Hutchings, F. King, I. P. Okoye, M. B. Padley, C. H. Rochester, *J Catal*, 1994, **148**, 464-469.